PROCEEDINGS OF THE ROYAL SOCIETY A

Proc. R. Soc. A (2011) **467**, 2209–2223
doi:10.1098/rspa.2010.0617
Published online 23 February 2011

A mechanism for enhanced static sliding resistance owing to surface waviness

By J. F. Waters and P. R. Guduru*

School of Engineering, Brown University, Providence, RI 02912, USA

This paper presents an analysis of static sliding resistance of a rigid sphere on a soft elastic material with axisymmetric waviness. When the sphere is loaded laterally under a fixed normal force, the contact area is subjected to mixed-mode loading. It is shown that, as the lateral loading increases, the decrease in contact area involves unstable jumps; and each unstable jump dissipates mechanical energy. The additional energy dissipation increases the peak force required for gross sliding of the interface compared with that of a flat surface. Thus, a mechanism is proposed for enhanced static sliding resistance on the surface of a soft material owing to surface waviness-induced instabilities. Such an increase in sliding resistance is analogous to a similar increase in the detachment force between a sphere and a wavy surface during normal separation, which was reported elsewhere. The influence of mode-mixity-dependent work of adhesion on the static sliding resistance of a wavy surface is also considered.

Keywords: wavy surface; sliding resistance; contact mechanics; bioinspired adhesion; friction

1. Introduction

As researchers work to design and fabricate reversible adhesive systems as effective as the biological attachment systems that have evolved naturally, it has been observed that surface structures which enhance adhesion also significantly enhance sliding resistance. Examples include the polyurethane fibrillar, spatulate-terminated structures studied by Kim *et al.* (2007), which sustained a 1.25–2.8× higher maximum static friction load than that measured on a flat control surface; the vertically aligned carbon nanotube arrays studied by Ge *et al.* (2007), which demonstrated a 6× enhancement in maximum static friction load; the polypropylene fibrillar structures studied by Majidi *et al.* (2006), which generated an order of magnitude enhancement in maximum static friction load; and the polydimethylsiloxane (PDMS) fibrillar, film-terminated structures studied by Yao *et al.* (2008) and Shen *et al.* (2008*a*,*b*), which showed a 1.8× and 10× enhancement in maximum static friction load, respectively. The energy dissipation mechanisms that enhance the adhesion of such structures are probably responsible for

*Author for correspondence (pradeep_guduru@brown.edu).

Received 28 November 2010
Accepted 17 January 2011

these concurrent enhancements in static sliding resistance as well. Glassmaker *et al.* (2007), Noderer *et al.* (2007) and Shen *et al.* (2008*a*,*b*) demonstrated that the energy dissipation resulting from crack trapping between fibrils can cause significant adhesion enhancement for film-terminated fibrillar structures. Surfaces containing patterns of incisions (Ghatak *et al.* 2004; Chung & Chaudhury 2005) or step discontinuities in height (Kendall 1975; Crosby *et al.* 2005) have also been shown to increase the fracture toughness of adhesive films through energy dissipation. More recent observations of enhanced adhesion and shearing resistance of biologically inspired structures include Glass *et al.* (2010), Unver & Sitti (2010), Murphy *et al.* (2009), Nadermann *et al.* (2010), Vajpayee *et al.* (2010) and Shen *et al.* (2009).

Guduru (2007), Guduru & Bull (2007) and Waters *et al.* (2009) showed that energy dissipation also leads to enhanced adhesion for soft elastic wavy surfaces through interface toughening and strengthening. The objective of this paper is to investigate the hypothesis that the mechanisms responsible for the enhanced adhesion of such wavy surfaces would also cause enhanced static sliding resistance. To this end, the behaviour of axisymmetric wavy surfaces subjected to tangential loading in the presence of adhesion is studied by extending the analytical contact mechanics model for pure adhesive normal loading (Waters *et al.* 2009), to include mixed normal and tangential loading, similar to the analysis for flat surfaces described in Waters & Guduru (2010). The goal of this investigation is to better understand the role of surface geometry in energy dissipation mechanisms, by using an idealized wavy geometry as a model system. Alternatively, a plane strain analysis could be performed based on the solution presented in Guduru (2007); however, the results are expected to be qualitatively similar. Axisymmetric wavy surfaces are clearly not seen in nature, but have advantages over three-dimensional wavy geometries for modelling purposes. Tangential loading can be readily incorporated into such a model, and the use of an axisymmetric geometry allows the significant body of literature on spherical single asperity adhesion and sliding to be drawn upon. It is also straightforward to include the results of Waters & Guduru (2010) on mode-mixity-dependent work of adhesion in the wavy surface contact model, which allows dissipative effects seen in the contact of soft elastomers or biological materials to be captured. The resulting analytical model predicts that the maximum static sliding resistance is amplified for a rigid spherical indenter in contact with a soft wavy surface, and the enhancement can be mapped for a range of geometries and material properties using the dimensionless parameters introduced in Waters *et al.* (2009). Geometry-induced energy dissipation is seen to result from unstable jumps in contact area during displacement-controlled lateral sliding of the wavy surface. Including mode-mixity-dependent work of adhesion in the model leads to an even higher prediction for sliding resistance.

The paper is organized as follows. In §2, a model is presented for the combined normal/tangential loading of an elastic axisymmetric wavy surface in contact with a rigid spherical punch, and essential dimensionless parameters for the problem are introduced. In §3, results for the evolution of contact area and lateral displacement with applied tangential loading, the enhancement in static sliding resistance for a range of wavy surface geometries and the effect of a mode-mixity-dependent work of adhesion are discussed.

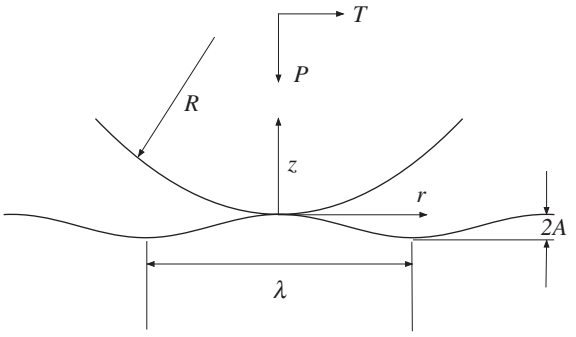

Figure 1. Geometry of the contact problem. A wavy surface with wavelength λ and amplitude A is indented by a rigid sphere of radius R under applied normal load P and tangential load T. Amplitude and wavelength are exaggerated in this diagram for visual clarity; in this model, $\lambda \ll R$ so that contact with multiple peaks is achieved.

2. Axisymmetric wavy surface contact under combined normal and tangential loading

(*a*) *Contact model*

In the following analysis, contact between the axisymmetric wavy surface of an elastic half-space and a rigid spherical indenter subjected to both normal and tangential loading in the presence of adhesion is modelled by building on the solutions presented by Waters *et al.* (2009), Waters & Guduru (2010) and Johnson (1997). The key assumptions are that complete contact is achieved within the contact area between the sphere and the wavy surface during loading; the normal and tangential tractions are uncoupled; and that slip is negligible within the contact area.

The geometry of the wavy surface contact problem is shown in figure 1, where the profile of the rigid sphere of radius R is approximated by the paraboloid

$$z = \frac{r^2}{2R}, \tag{2.1}$$

and the height of the wavy surface is described as a sinusoidal function of the radial coordinate r,

$$z = A\left(1 - \frac{\cos 2\pi r}{\lambda}\right), \tag{2.2}$$

where A and λ are the amplitude and wavelength of waviness, respectively. When $A > 0$, the surface is convex up at $r = 0$; when $A < 0$, the surface is centrally concave. In this model, it is assumed $\lambda \ll R$ so that the initial contact area consists of multiple wavelengths.

From Waters *et al.* (2009), the relationship between the applied normal load P and contact radius a for the axisymmetric wavy surface contact problem in the presence of Johnson–Kendall–Roberts (JKR) adhesion (Johnson *et al.* 1971) is

$$P(a) = P_1(a) - \sqrt{8\pi E^* w a^3}, \tag{2.3}$$

where w is the work of adhesion and the Hertz contact load $P_1(a)$ for the wavy surface is

$$P_1(a) = 2E^* \left[\left(\frac{2}{R} + \frac{4\pi^2 A}{\lambda^2} \right) \frac{a^3}{3} + \frac{\pi A a}{2} H_1\left(\frac{2\pi a}{\lambda} \right) - \frac{\pi^2 A a^2}{\lambda} H_2\left(\frac{2\pi a}{\lambda} \right) \right]. \quad (2.4)$$

Here, $E^* = E/(1-\nu^2)$ is the plane strain modulus of the elastic solid, where E is the elastic modulus, ν is Poisson's ratio and $H_n(\cdot)$ is the Struve function of order n (see Abramowitz & Stegun 1965). (Note that equation (2.4) reduces to the Hertz solution for a sphere in contact with a flat half-space, $P_1 = 4E^* a^3/(3R)$, when $A = 0$.) The normal contact pressure $p(r)$ for this geometry is given by

$$p(r) = p_1(r) - \frac{P_1 - P}{2\pi a^2 \sqrt{1 - \frac{r^2}{a^2}}}, \quad (2.5)$$

where $p_1(r)$ is given by

$$p_1(r) = \frac{E^*}{\pi} \left[\left(\frac{2}{R} + \frac{4\pi^2 A}{\lambda^2} \right) \sqrt{a^2 - r^2} + \frac{\pi^2 A}{\lambda} \int_r^a \frac{H_0\left(\frac{2\pi\alpha}{\lambda}\right)}{\sqrt{\alpha^2 - r^2}} \mathrm{d}\alpha \right.$$
$$\left. - \frac{2\pi^3 A}{\lambda^2} \int_r^a \frac{\alpha H_1\left(\frac{2\pi\alpha}{\lambda}\right)}{\sqrt{\alpha^2 - r^2}} \, \mathrm{d}\alpha \right]. \quad (2.6)$$

The mode I stress intensity factor at the contact boundary, following Maugis & Barquins (1978), is defined as

$$K_I = \frac{P_1 - P}{2a\sqrt{\pi a}}. \quad (2.7)$$

It is assumed that the amplitude of surface waviness is sufficiently small (compared with the wavelength) such that the tangential traction distribution $q(r)$ within the area of contact can be approximated as being the same as that for a sphere in no-slip contact with a flat half-space, given by Johnson (1985) as

$$q(r) = \frac{T}{2\pi a^2 \sqrt{1 - (r^2/a^2)}}, \quad (2.8)$$

where T is the applied tangential force. The assumption also enables superposition of the elasticity solutions owing to normal loading and tangential loading. In order to relate the critical tangential force to the applied normal force and the work of adhesion, we follow the general procedure of Johnson (1997). From equation (2.8), the modes II and III stress intensity factors around the contact edge can be written as

$$K_{\mathrm{II}\theta} = \frac{T}{2a\sqrt{\pi a}} \cos\theta \quad \text{and} \quad K_{\mathrm{III}\theta} = \frac{T}{2a\sqrt{\pi a}} \sin\theta, \quad (2.9)$$

where θ is the angle between the radius vector and the direction of T. The energy release rate along the contact periphery can then be expressed as

$$G = \frac{1}{2E^*} \left[K_{\mathrm{I}}^2 + K_{\mathrm{II}\theta}^2 + \frac{1}{1-\upsilon} K_{\mathrm{III}\theta}^2 \right]. \quad (2.10)$$

To remove the cumbersome θ dependence of the above equation, averaging the stress intensity factors around the periphery of the contact area results in the expression

$$G = \frac{1}{2E^*}\left[K_{\mathrm{I}}^2 + \frac{2-\nu}{2-2\nu}K_{\mathrm{II}}^2\right], \tag{2.11}$$

with effective stress intensity factor

$$K_{\mathrm{II}} = \frac{T}{2a\sqrt{\pi a}}. \tag{2.12}$$

To find a relation between the contact radius a and the applied loads P and T, the energy release rate is set equal to the work of adhesion. Setting $G = w$ and combining equations (2.7), (2.11) and (2.12) results in the solution

$$w = \frac{1}{8\pi E^* a^3}\left[(P_1 - P)^2 + \frac{2-\nu}{2-2\nu}T^2\right]. \tag{2.13}$$

If the applied normal load P is held constant during the tangential loading, equation (2.13) can be rearranged to obtain an expression for the relationship between tangential load and contact radius,

$$T = \left[\frac{2-2\nu}{2-\nu}(8\pi E^* w a^3 - (P_1 - P)^2)\right]^{1/2}, \tag{2.14}$$

where P_1 is dependent upon a through equation (2.4). A similar expression was obtained by Savkoor & Briggs (1977) in an analysis of the effect of tangential force on the contact of elastic solids in adhesion by minimizing the total potential energy under the combined action of normal and tangential loads. Since their procedure did not involve mode averaging around the periphery, their expression did not contain the Poisson ratio term in equation (2.14). Finally, the uniform lateral tangential shift of the two contacting bodies, with negligible slip on the contact area, is given by Mindlin (1949) as

$$\delta = \frac{1}{2}\left(\frac{2-\nu}{2-2\nu}\right)\frac{T}{E^* a}, \tag{2.15}$$

assuming once again that this classical tangential loading result for a sphere on a flat surface gives a close approximation for the case of small amplitude surface waviness. Equations (2.14) and (2.15) together provide relationships between the tangential load T, contact radius a and lateral shift δ for a known normal load P.

(*b*) *Mode-mixity-dependent work of adhesion*

For the case of pure normal loading presented in Waters *et al.* (2009), it was assumed that the work of adhesion w remained constant during the detachment process. However, as discussed in Waters & Guduru (2010), experimental evidence shows that, under combined normal and tangential loading, w is strongly dependent upon mode mixity for materials with interfacial dissipation during contact, such as viscoelastic materials. Hence, it is desirable to allow w to be dependent upon mode mixity so as to capture some aspects of viscoelastic behaviour within this wavy surface contact model. To incorporate the

experimental measurements of w from Waters & Guduru (2010), parametrization similar to that of Hutchinson & Suo (1992) is used to express the mode-mixity-dependent work of adhesion as

$$w(\psi) = w_0 \xi(\psi) = w_0 \left(1 + \frac{2-\nu}{2-2\nu} \tan^2[(1-\Lambda)\psi]\right), \tag{2.16}$$

where w_0 is the work of adhesion for pure mode I loading and ψ is the phase angle of mode mixity, defined as

$$\psi = \tan^{-1}\left(\frac{K_{\mathrm{II}}}{K_{\mathrm{I}}}\right). \tag{2.17}$$

The parameter Λ in equation (2.16) determines the influence of mode mixity, and is bounded by $0 \le \Lambda \le 1$. If $\Lambda = 1$, $w(\psi) = w_0$ for all ψ, which is the classical surface energy criterion. If $\Lambda = 0$, the crack is fully shielded from any effects of mode II and crack advance depends only upon the mode I component. Hence, the $\Lambda = 0$ case is often referred to as being K_{II} independent. This can be seen by noting that, when equations (2.16) and (2.17) are substituted into equation (2.11), K_{II} drops out of the resulting fracture criterion, leaving behind K_{I} only.

(*c*) *Dimensionless parametrization*

The following non-dimensional parameters are introduced to represent the above results in a more useful form:

$$\alpha = \frac{AR}{\lambda^2} \quad \text{and} \quad \beta = \left(\frac{\lambda}{R}\right)^3 \frac{E^* R}{2\pi w_0}, \tag{2.18}$$

where α represents the degree of surface waviness; larger values of α correspond to surfaces with high-amplitude, short wavelength waviness, whereas smaller values of α correspond to surfaces with shallow, long wavelength waviness. β provides a measure of the relative stiffness of the material with respect to its surface energy; small β values correspond to more compliant materials where surface energy effects are more dominant, whereas large β values correspond to stiffer materials where surface energy is less dominant. In addition to α and β, the dimensionless loads, contact radius and lateral displacement are defined as

$$\bar{P} = \frac{P}{\pi w_0 R}, \quad \bar{T} = \frac{T}{\pi w_0 R}, \quad \bar{a} = \frac{a}{\lambda}, \quad \bar{\delta} = \frac{\delta R}{\lambda^2}, \tag{2.19}$$

respectively. Substituting equations (2.18) and (2.19) into equations (2.14) and (2.15) and using $\nu = 0.5$ for an incompressible material, the following expressions for dimensionless tangential load $\bar{T}$ and lateral shift $\bar{\delta}$ are obtained:

$$\bar{T} = \left[\frac{2}{3}(16\beta\xi(\psi)\bar{a}^3 - (\bar{P}_1 - \bar{P})^2)\right]^{1/2} \tag{2.20}$$

and

$$\bar{\delta} = \frac{3}{8}\frac{\bar{T}}{\beta\bar{a}}, \tag{2.21}$$

where $\bar{P}_1 = (\bar{P}_1/\pi w_0 R)$. $\xi(\psi)$ is defined as in equation (2.16), and from equations (2.7), (2.12) and (2.17), the phase angle can be expressed as

$$\psi = \tan^{-1}\left(\frac{\bar{T}}{\bar{P}_1(\bar{a}) - \bar{P}}\right), \tag{2.22}$$

in terms of the dimensionless parameters. For $\Lambda = 1$, $\xi(\psi) = 1$ and equations (2.20) and (2.21) give explicit expressions for $\bar{T}$ and $\bar{\delta}$ in terms of $\bar{a}$. This allows for the parametric iteration of $\bar{a}$ to obtain a relation between $\bar{T}$ and $\bar{\delta}$. For all other values of Λ, equation (2.20) is no longer an explicit expression for $\bar{T}$ because of its dependence on ψ. Hence, $\bar{T}$ must be solved numerically for each value of $\bar{a}$. In both cases, the dimensionless parametrization presented here allows for a comprehensive mapping of $\bar{T}$–$\bar{a}$ and $\bar{T}$–$\bar{\delta}$ for a given $\bar{P}$ in the parameter space of α and β.

3. Results and discussion

(*a*) *Enhancement of static sliding resistance for constant work of adhesion*

Before investigating the enhancement in static sliding resistance predicted by the axisymmetric wavy surface contact model, it is helpful to examine an example contact problem for a specific geometry for the classical surface energy criterion case, i.e. $\Lambda = 1$ and $w = w_0$. Figure 2*a* shows the variation of normal load $\bar{P}$ with normal displacement $\bar{\Delta}$ for $\beta = 0.1$, computed using the results in §2. The $\alpha = 0$ curve corresponds to the case of a sphere in contact with a flat surface, which is shown for reference, whereas the $\alpha = 0.2$ case corresponds to a wavy geometry. Before applying a tangential load, the normal displacement of the sphere is controlled so that the surface is loaded in net compression and then unloaded to a specific value of $\bar{P}$ and held fixed there, as illustrated by the arrows in figure 2*a*. In the specific case shown in figure 2, unloading is stopped when $\bar{P} = 0$, and it is held constant during the subsequent tangential loading. Figure 2*b* shows the corresponding $\bar{P}$–$\bar{a}$ plot for the normal loading; the value of $\bar{a}$ when $\bar{P} = 0$ becomes the initial contact radius for the tangential loading that follows. Figure 2*c* shows the relation between the applied tangential load $\bar{T}$ and the corresponding lateral shift $\bar{\delta}$. First consider the flat surface case, which is similar to that described by Savkoor & Briggs (1977), Savkoor (1987) and Johnson (1997). As $\bar{\delta}$ increases, $\bar{T}$ increases monotonically, until a maximum is reached (point A), beyond which it begins to decrease. In a load-controlled experiment, the point A represents the maximum static sliding resistance, where spontaneous detachment takes place. In a displacement-controlled experiment, detachment occurs at B, where the tangent is vertical. Now, consider the case of sliding a sphere on a wavy surface in a displacement-controlled experiment; in figure 2*c*, at point C, further increase in $\bar{\delta}$ results in a spontaneous drop in the load to point D, which is the next available equilibrium position, and a corresponding drop in the contact radius as shown in figure 2*d*. Subsequent increase in $\bar{\delta}$ takes $\bar{T}$ to point F, where it experiences the next unstable drop. Thus, sliding takes place in a series of unstable drops in $\bar{T}$ and $\bar{a}$. Each unstable drop in $\bar{T}$ dissipates

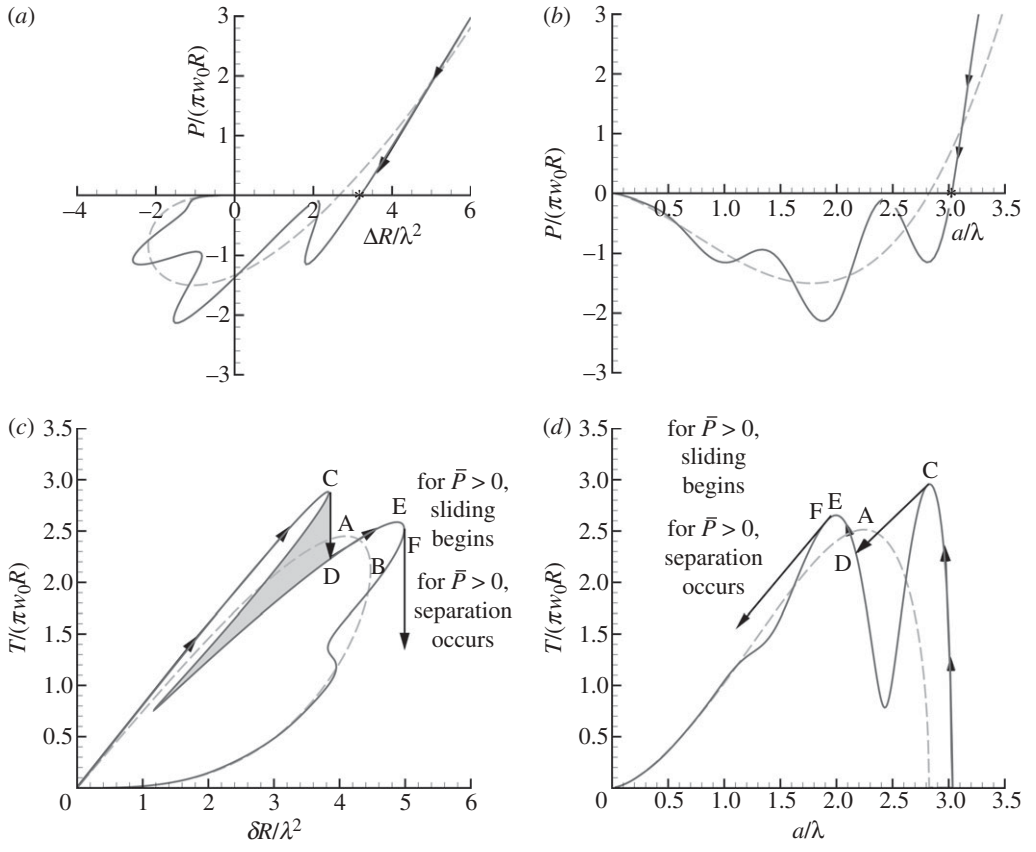

Figure 2. Illustration of loading process for $\alpha = 0$ (flat surface) and $\alpha = 0.2$. Solution for the flat surface is shown in dashed lines for comparison. A normal load is applied first, followed by a tangential load. (*a*) Surface is pressed into full contact and then unloaded to a fixed normal load (in this case, $\bar{P} = 0$, denoted by the asterisk on the abscissa). For more details of the normal loading case, see Guduru (2007). (*b*) The contact radius $\bar{a}$ at the final value of $\bar{P}$ determines the initial contact radius at the onset of tangential loading. (*c*) Under displacement-controlled tangential loading, $\bar{T}$ undergoes unstable jumps, resulting in mechanical energy dissipation, represented by the shaded area. (*d*) As the tangential loading increases, the contact radius decreases from its initial value and jumps to lower values in correspondence with the instabilities seen in (*c*). Although $\bar{P} = 0$ for the plots shown, in (*c*) and (*d*) the notes regarding sliding versus separation for $\bar{P} > 0$ and $\bar{P} < 0$, respectively, refer to the expected event at the corresponding unstable point when the normal load in non-zero. (*a*,*b*) Dashed line, $\alpha = 0$; solid line, $\alpha = 0.2$; $\beta = 0.1$. (*c*) Dashed line, $\alpha = 0$; solid line, $\alpha = 0.2$; grey colour, dissipated energy; $\bar{P} = 0$; $\beta = 0.1$. (*d*) Dashed line, $\alpha = 0$; solid line, $\alpha = 0.2$; $\bar{P} = 0$; $\beta = 0.1$.

mechanical energy; in figure 2*c*, the energy dissipation during the C–D jump is the shaded area next to it. Hence, the geometry-induced instabilities during sliding on a wavy surface result in greater energy dissipation than that for a flat surface. This phenomenon is analogous to similar instabilities reported in Guduru (2007) and Waters *et al.* (2009) during normal detachment from a wavy surface. Further, note that, as a consequence of the additional energy dissipation, the maximum sliding resistance for the wavy surface, i.e. the tangential load at point

C, is greater than that for a flat surface, point A. Thus, the geometry-induced instabilities enhance the static sliding resistance, which is again analogous to a similar increase in the detachment force discussed in Guduru (2007) and Waters *et al.* (2009). The magnitude of the enhancement depends on the non-dimensional parameters α and β, and is measured by the variable

$$\hat{T} = \frac{(\bar{T}_{\max})_{\text{wavy}}}{(\bar{T}_{\max})_{\text{flat}}}. \tag{3.1}$$

At the maximum attainable value of $\bar{\delta}$ (point F in figure 2*c*), the limit of static equilibrium is reached. Beyond F, the portions of the equilibrium curves corresponding to smaller values of $\bar{a}$ are inaccessible. For compressive normal loading ($\bar{P} > 0$), the system transitions to full sliding and a no-slip model no longer applies. For tensile normal loading ($\bar{P} < 0$), sliding is not permissible and separation occurs. The specific details of slip transition are outside the scope of this model. The experimental results of Waters & Guduru (2010) indicate that the no-slip approximation is reasonable until a phase angle of $\psi \approx 60^\circ$ for flat PDMS, which was found to have a mode-mixity parameter $\Lambda = 0.15$. They also showed that, for increased tangential loading, the contact area no longer remains circular; however, the maximum tangential load sustainable by the contact interface prior to initiation of a slip event was always underpredicted by the model, by as much as 50 per cent. Hence, the present analytical model for wavy surfaces is also expected to underpredict the maximum static sliding resistance. The model presented here is intended to highlight the role of surface waviness in enhancing the sliding resistance, rather than provide a precise predictive tool that captures all the details of interfacial slip.

The effect of α and β on the model predictions is illustrated in figure 3, which shows $\bar{T}$–$\bar{\delta}$ and $\bar{T}$–$\bar{a}$ plots for $\bar{P} = 0$, $\beta = 0.1$, and four values of α. For the $\alpha = 0$ case (flat surface), the curves are continuous and smooth. For the $\alpha = 0.1$ case, the curves are still continuous but feature folds which, as noted above, cause energy dissipation during tangential loading. For $\alpha = 0.3$ and 0.5, not only are the folds sharper (indicating greater $\bar{T}_{\max}$), but the $\bar{T}$–$\bar{a}$ curves are no longer continuous; there are ranges of $\bar{a}$ for which no equilibrium load can be supported.

From a series of plots such as those shown in figure 3, the enhancement in peak static friction load $\hat{T}$ can be mapped for the parameters α and β. Figure 4*a* shows how $\hat{T}$ varies with α when $\bar{P} = 0$ for $\beta = 0.1$, 0.5 and 1. Kinks in the data curves occur at points where $\bar{T}$–$\bar{a}$ or $\bar{T}$–$\bar{\delta}$ solutions have a transition from being continuous to having a discontinuity. For most combinations of α and β, $\hat{T}$ increases with increasing $|\alpha|$, or higher amplitude, shorter wavelength surfaces. Also, in most cases, $\hat{T}$ increases with β for a fixed α. Although figure 4 suggests that $T_{\max}$ will continue to increase with α, in practice the maximum enhancement in static sliding resistance would be limited by the condition that the waviness must be shallow enough for complete contact to be maintained between the wavy surface and the rigid indenter, while, at the same time, λ must be small enough so that the wavy contact problem does not resemble single-asperity contact. For higher values of α (i.e. as the waviness gets deeper), even for $P = 0$ or $P > 0$, the normal stress at the troughs of the wavy interface can be tensile and exceed the interface strength, resulting in local interface detachment. This results in

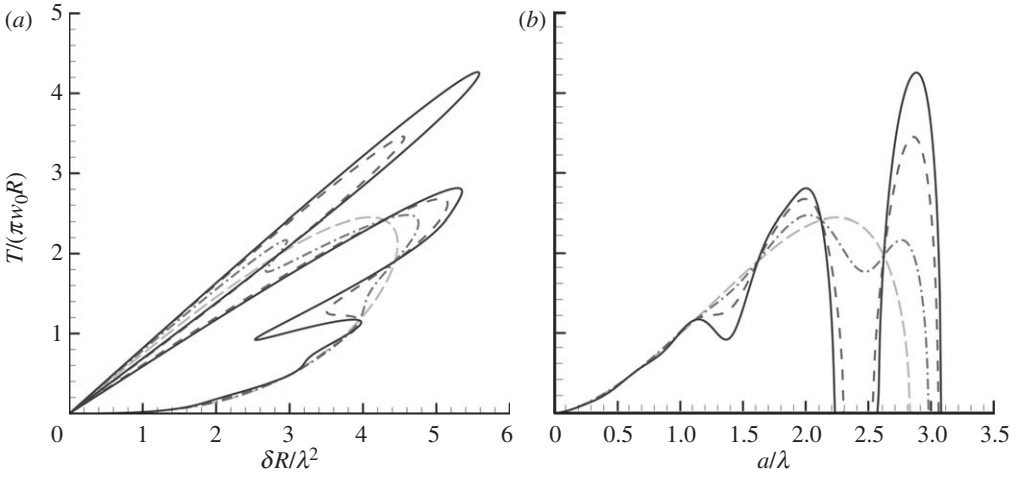

Figure 3. Equilibrium solution curves for $\bar{P}=0$, $\beta=0.1$ and $w=w_0$. (*a*) Normalized tangential loading versus lateral shift. (*b*) Normalized tangential loading versus contact area. (*a*,*b*) $\bar{P}=0$; $\beta=0.1$; grey dashed line, $\alpha=0$; dashed-dotted line, $\alpha=0.1$; black dashed line, $\alpha=0.3$; solid line, $\alpha=0.5$.

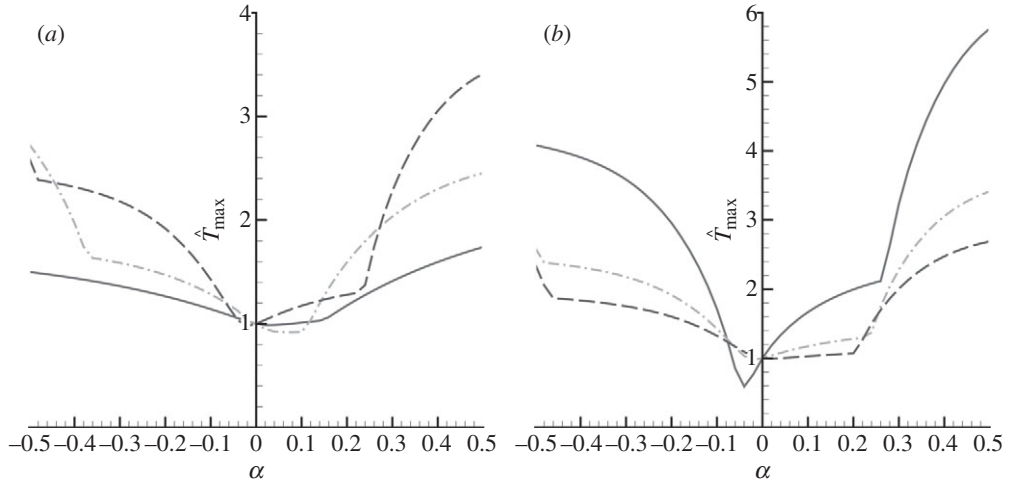

Figure 4. Predicted maximum static friction load enhancement $\hat{T}$ for (*a*) fixed $\bar{P}=0$ and a range of geometries; (*b*) fixed $\beta=1$ and a range of normal loads. (*a*) Solid line, $\beta=0.1$; dashed-dotted line, $\beta=0.5$; dashed line, $\beta=1$. (*b*) Solid line, $\bar{P}=-1$; dashed-doted line, $P=0$; dashed line, $\bar{P}=1$.

discontinuous contact (i.e. partial contacts of the wavy crests), for which case the model presented is not applicable. The ever increasing $T_{\max}$ with α is an artefact of linear elastic fracture mechanics, which does not consider the interface strength in the fracture criterion. A more detailed discussion of the limiting value of α is presented elsewhere (Guduru 2007; Waters & Guduru 2010; Waters *et al.* 2010). A range of validity of α for a particular material pair (PDMS and polycarbonate) can be obtained by considering the experimental data of Guduru & Bull (2007),

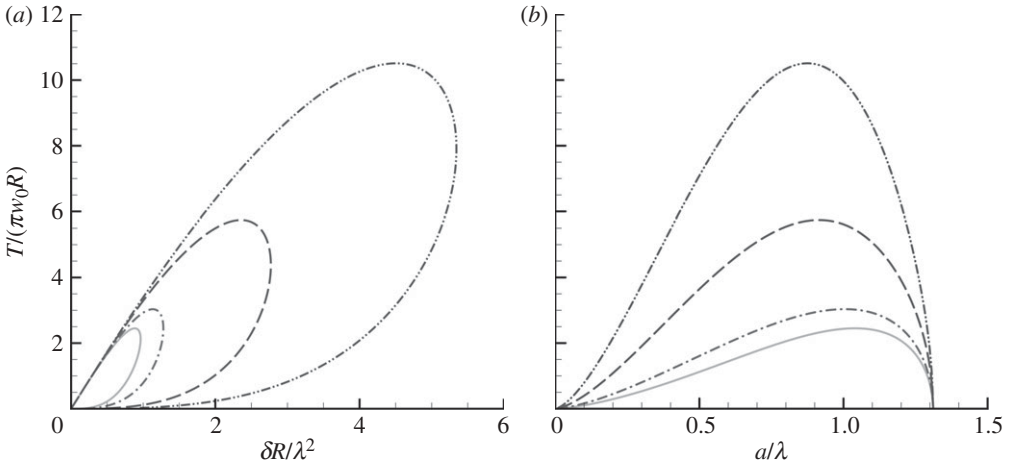

Figure 5. Equilibrium solution curves for mode-mixity-dependent work of adhesion with $\bar{P}=0$, $\alpha=0$ (flat surface) and $\beta=1$. (*a*) Normalized tangential loading versus lateral shift. (*b*) Normalized tangential loading versus contact area. (*a*,*b*) Solid line, $\Lambda=1$; grey dashed-dotted line, $\Lambda=0.5$; dashed line, $\Lambda=0.2$; black dashed-dotted line, $\Lambda=0.1$. $\bar{P}=0$; $\alpha=0$; $\beta=1$.

who investigated wavy surface adhesion. From table 1 of their work, the maximum value of α they employed was 1.25, which sets a lower bound in order to maintain full contact for their material system, which also extends to the results shown in figure 4. Figure 4*b* shows the effect of the normal load $\bar{P}$ on $\hat{T}$ for $\beta=1$; plots are shown for $\bar{P}=-1$, 0 and 1. As before, for most combinations, $\hat{T}$ increases with increasing $|\alpha|$. $\hat{T}$ also tends to increase for decreasing $\bar{P}$. Physically, this means that a wavy surface is predicted to enhance static sliding resistance more significantly under tensile normal loading than under compressive loading. The asymmetry of the shape of the plots with respect to the sign of α (i.e. the sign of A) is primarily an artefact of higher values of β, which implies that there are only a few waves in the contact area. The sign of A (i.e. the half-space is concave or convex at $r=0$) makes a significant difference only when the number of waves in the contact area is small, fewer than five for instance. When the number of waves in the contact area is large, i.e. small values of β, the asymmetry gets smaller, as indicated by the $\beta=0.1$ case in figure 4*a*. The main conclusion from the foregoing analysis is that the waviness-induced instabilities enhance the lateral sliding resistance, just as they tend to increase the adhesion strength during normal separation. Depending on the non-dimensional parameter values, the enhancement can be several times that corresponding to the flat surface. Hence, we propose that it is a mechanism for increase in sliding resistance for rough elastomeric surfaces.

(*b*) *Enhancement of static sliding resistance for mode-mixity-dependent work of adhesion*

Introducing mode-mixity dependence into the work of adhesion has significant consequences for the predicted peak tangential static loading. Figure 5 displays sample results for a flat surface ($\alpha=0$) for the representative case of $\bar{P}=0$, $\beta=1$.

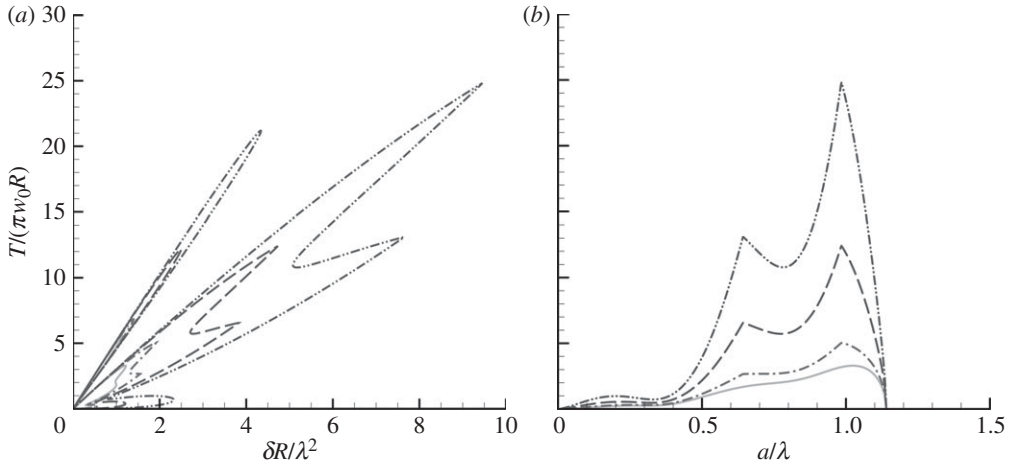

Figure 6. Equilibrium solution curves for mode-mixity-dependent work of adhesion with $\bar{P}=0$, $\alpha=0.3$ and $\beta=1$. (*a*) Normalized tangential loading versus lateral shift. (*b*) Normalized tangential loading versus contact area. Solid line, $\Lambda=1$; grey dashed-dotted line, $\Lambda=0.5$; dashed line, $\Lambda=0.2$; black dashed-dotted line, $\Lambda=0.1$. $\bar{P}=0$; $\alpha=0$; $\beta=1$.

Increasing the influence of mode mixity upon the work of adhesion by decreasing Λ in equation (2.16) has the effect of expanding the $\bar{T}-\bar{\delta}$ and $\bar{T}-\bar{a}$ envelopes, significantly raising the maximum sustainable tangential force, as expected. Figure 6 shows the effect of changing Λ on the equilibrium solution curves for a wavy surface, for $\alpha=0.3$. Again, decreasing Λ is seen to expand the solution envelopes and significantly amplify the peak tangential loads, enhancing static sliding resistance. Decreasing Λ, therefore, also increases the amount of available energy to be dissipated during unstable jumps in $\bar{T}$ under displacement-controlled loading, further toughening the contact interface.

The strong influence of the parameter Λ upon the peak sustainable tangential load $\bar{T}_{\max}$ for the representative case $\bar{P}-0$, $\beta=1$ is shown in figure 7*a*. As $\Lambda\to 0$, $\bar{T}_{\max}$ rises sharply. When $\Lambda=0$, $\hat{T}_{\max}\to\infty$ for both the wavy and flat surface cases, as $w\to\infty$ for $\psi=90^\circ$. The predicted enhancement in static friction $\hat{T}$ for the wavy surface is shown in figure 7*b* for $\Lambda>0$. At the limit $\Lambda=1$ ($w=w_0$), increasing α generates enhancement in static sliding resistance through geometry alone, as discussed in §3*a* and illustrated in figure 4. However, for lower values of Λ, additional enhancement in sliding resistance is seen, which is above and beyond the waviness effect. Decreasing Λ corresponds to increasing the effective energy dissipation in the model. The experimental results of Waters & Guduru (2010) for a rigid sphere subjected to combined normal and tangential loading on a flat PDMS surface indicated that $\Lambda=0.15$ provided a good fit to the measured work of adhesion. For this Λ, the predicted $\hat{T}$ seen for the range of α presented in figure 7*b* for $\bar{T}=0$, $\beta=1$ falls into the range of peak static friction load enhancement reported by other researchers (up to a factor of 4), as discussed in §1. For example, consider the case of $\alpha=0.2$, a rigid sphere of radius 5 mm in contact with an axisymmetric wavy PDMS surface with $E^*=1\,\mathrm{MPa}$, $w_0=50\,\mathrm{mJ\,m^{-2}}$, $\lambda=0.2\,\mathrm{mm}$ and $A=1.6\,\mu\mathrm{m}$; the predicted enhancement in maximum static friction load

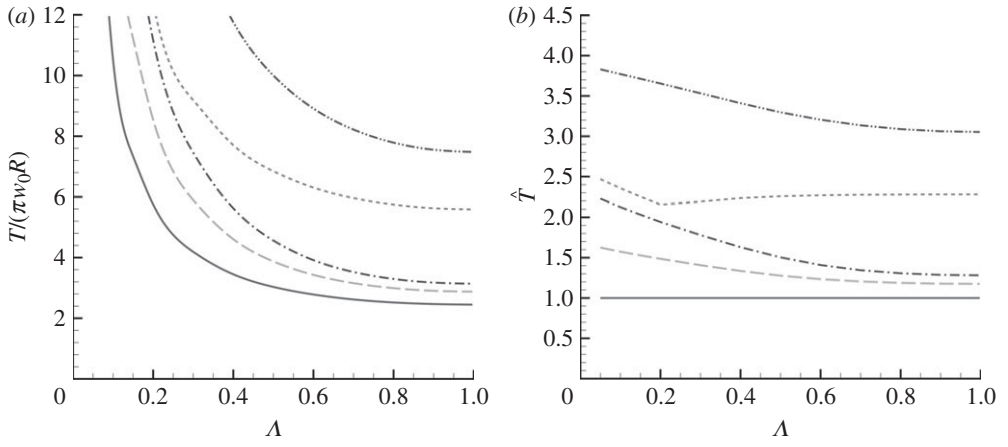

Figure 7. Predicted enhancement of static sliding resistance for mode-mixity-dependent work of adhesion. (*a*) Maximum tangential load as a function of Λ. (*b*) Magnitude of static friction enhancement $\hat{T}$ seen for the wavy surface compared with a flat surface, as a function of Λ. Significant increases in static friction are seen as $\Lambda \to 0$. (*a*,*b*) Solid line, $\alpha = 0$; grey dashed line, $\alpha = 0.1$; grey dashed-dotted line, $\alpha = 0.2$; black dashed line, $\alpha = 0.3$; black dashed-dotted line, $\alpha = 0.4$. $\bar{P} = 0$; $\beta = 0.1$.

would be two times that of a flat surface. In short, these results indicate that significant enhancement in static sliding resistance is attainable through the introduction of surface waviness, and the peak static friction loads are further enhanced for interfaces with mode-mixity-dependent work of adhesion. Rand & Crosby (2009) recently carried out an experimental investigation of friction of wrinkled elastomers, in which they prepared elastomeric surfaces with parallel wrinkles and measured the sliding resistance parallel and perpendicular to the wrinkles and compared it with that of a reference flat surface. Their results indicated that the surface showed least frictional resistance when the sliding direction was normal to the wrinkles. However, in their experiments, only the wrinkle crests were in contact with the sliding glass sphere. Since the solution used in this paper (equations (2.3)–(2.8)) is based on full contact over a circular area of radius a, the model presented here is not applicable to interpret their results. A separate model that considers partial contact with multiple crests and considers the equilibrium of each of the many crack tips needs to be developed to analyse experiments similar to those of Rand & Crosby (2009). However, in their experiments, reducing the wrinkle amplitude and applying initial compression in their experiments will ensure full initial contact over a central region, which will present an opportunity to examine the predictions of the model presented here.

4. Summary

A possible mechanism is proposed for enhancement in static sliding resistance owing to surface waviness-induced instabilities in soft materials. In order to quantify the proposed mechanism, a model is presented for an axisymmetric wavy surface in contact with a rigid sphere subjected to combined normal and

tangential loading in the presence of JKR adhesion. Wavy surfaces are expected to increase the maximum sustainable static sliding resistance by strengthening the interface via higher peak sustainable tangential loads, as well as toughening the interface through energy dissipation. Enhancements in detachment strength and toughness owing to surface waviness were demonstrated by Guduru (2007) and Waters *et al.* (2009); this paper extends these results to tangential sliding. A mode-mixity-dependent work of adhesion was used to predict the static sliding resistance of viscoelastic elastomers or biological materials, as indicated by the experimental results presented in Waters & Guduru (2010). When the work of adhesion increases with the degree of mode mixity, the maximum static friction loads are predicted to surpass those sustained by the wavy geometry when the work of adhesion remains constant. Thus, the combination of geometry and dissipative materials allows significant enhancement in static sliding to be achieved. Important future work includes experimental verification of the model predictions and extending the analysis to three-dimensional surface roughness.

This work was supported by the Mechanics of Multifunctional Materials and Microsystems programme of the Air Force Office of Scientific Research (grant no. FA9550-05-1-0210; programme manager, Dr Les Lee) and the National Science Foundation (grant no. CMS-0547032).

References

Abramowitz, M. & Stegun, I. A. 1965 *Handbook of mathematical functions with formulas, graphs, and mathematical tables*. New York, NY: Dover.

Chung, J.-Y. & Chaudhury, M. K. 2005 Roles of discontinuities in bio-inspired adhesive pads. *J. R. Soc. Interface* **2**, 55–61. (doi:10.1098/rsif.2004.0020)

Crosby, A. J., Hageman, M. & Duncan, A. 2005 Controlling polymer adhesion with 'pancakes'. *Langmuir* **21**, 11 738–11 743. (doi:10.1021/la051721k)

Ge, L., Sethi, S., Ci, L., Ajayan, P. M. & Dhinojwala, A. 2007 Carbon nanotube-based synthetic gecko tapes. *Proc. Natl Acad. Sci. USA* **104**, 10 792–10 795. (doi:10.1073/pnas.0703505104)

Ghatak, A., Mahadevan, L., Chung, J. Y., Chaudhury, M. K. & Shenoy, V. 2004 Peeling from a biomimetically patterned thin elastic film. *Proc. R. Soc. Lond. A* **460**, 2725–2735. (doi:10.1098/rspa.2004.1313)

Glass, P., Hoyong, C., Washburn, N. R. & Sitti, M. 2010 Enhanced wet adhesion and shear of elastomeric micro-fiber arrays with mushroom tip geometry and a photopolymerized p(DMA-co-MEA) tip coating. *Langmuir* **26**, 17 357–17 362. (doi:10.1021/la1029245)

Glassmaker, N. J., Jagota, A., Hui, C.-Y., Noderer, W. L. & Chaudhury, M. K. 2007 Biologically inspired crack trapping for enhanced adhesion. *Proc. Natl Acad. Sci. USA* **104**, 10 786–10 791. (doi:10.1073/pnas.0703762104)

Guduru, P. R. 2007 Detachment of a rigid solid from an elastic wavy surface: theory. *J. Mech. Phys. Solids* **55**, 445–472. (doi:10.1016/j.jmps.2006.09.004)

Guduru, P. R. & Bull, C. 2007 Detachment of a rigid solid from an elastic wavy surface: experiments. *J. Mech. Phys. Solids* **55**, 473–488. (doi:10.1016/j.jmps.2006.09.007)

Hutchinson, J. W. & Suo, Z. 1992 Mixed mode cracking in layered materials. In *Advances in applied mechanics*, vol. 29 (eds J. W. Hutchinson & T. Y. Wu), pp. 63–191. Boston, MA: Academic Press.

Johnson, K. L. 1985 *Contact mechanics*. Cambridge, UK: Cambridge University Press.

Johnson, K. L. 1997 Adhesion and friction between a smooth elastic spherical asperity and a plane surface. *Proc. R. Soc. Lond. A* **453**, 163–179. (doi:10.1098/rspa.1997.0010)

Johnson, K. L., Kendall, K. & Roberts, A. D. 1971 Surface energy and the contact of elastic solids. *Proc. R. Soc. Lond. A* **324**, 301–313. (doi:10.1098/rspa.1971.0141)

Kendall, K. 1975 Control of cracks by interfaces in composites. *Proc. R. Soc. Lond. A* **341**, 409–428. (doi:10.1098/rspa.1975.0001)

Kim, S., Aksak, B. & Sitti, M. 2007 Enhanced adhesion of elastomer microfiber adhesives with spatulate tips. *Appl. Phys. Lett.* **91**, 221913. (doi:10.1063/1.2820755)

Majidi, C. *et al.* 2006 High friction from a stiff polymer using microfiber arrays. *Phys. Rev. Lett.* **97**, 076103. (doi:10.1103/PhysRevLett.97.076103)

Maugis, D. & Barquins, M. 1978 Fracture mechanics and the adherence of viscoelastic bodies. *J. Phys. D Appl. Phys.* **11**, 1989–2023. (doi:10.1088/0022-3727/11/14/011)

Mindlin, R. D. 1949 Compliance of elastic bodies in contact. *J. Appl. Mech.* **16**, 259.

Murphy, M. P., Kim, S. & Sitti, M. 2009 Enhanced adhesion by gecko-inspired hierarchical fibrillar adhesives. *ACS Appl. Mater. Interfaces* **1**, 849–855. (doi:10.1021/am8002439)

Nadermann, N., Ning, J., Jagota, A. & Hui, C. Y. 2010 Active switching of adhesion in a film-terminated fibrillar structure. *Langmuir* **26**, 15 464–15 471. (doi:10.1021/la102593h)

Noderer, W. L., Shen, L., Vajpayee, S., Glassmaker, N. J., Jagota, A. & Hui, C.-Y. 2007 Enhanced adhesion and compliance of film-terminated fibrillar structures. *Proc. R. Soc. A* **463**, 2631–2654. (doi:10.1098/rspa.2007.1891)

Rand, C. J. & Crosby, A. J. 2009 Friction of soft elastomeric wrinkled surfaces. *J. Appl. Phys.* **106**, 064913. (doi:10.1063/1.3226074)

Savkoor, A. R. 1987 Dry adhesive contact of elastomers. Master's thesis, Delft University of Technology, Delft, The Netherlands.

Savkoor, A. R. & Briggs, G. A. D. 1977 The effect of tangential force on the contact of elastic solids in adhesion. *Proc. R. Soc. Lond. A* **356**, 103–114. (doi:10.1098/rspa.1977.0123)

Shen, L., Glassmaker, N. J., Jagota, A. & Hui, C.-Y. 2008*a* Strongly enhanced static friction using a film-terminated fibrillar interface. *Soft Matter* **4**, 618–621. (doi:10.1039/b714737f)

Shen, L., Hui, C.-Y. & Jagota, A. 2008*b* A two-dimensional model for enhanced adhesion of film-terminated fibrillar structures by crack trapping. *J. Appl. Phys.* **104**, 123506. (doi:10.1063/1.3035908)

Shen, L. L., Jagota, A. & Hui, C. Y. 2009 Mechanism of sliding friction on a film-terminated fibrillar interface. *Langmuir* **25**, 2772–2780. (doi:10.1021/la803390x)

Unver, O. & Sitti, M. 2010 Flat dry elastomer adhesives as attachment materials for climbing robots. *IEEE Trans. Robot.* **26**, 131–141. (doi:10.1109/TRO.2009.2033628)

Vajpayee, S., Jagota, A. & Hui, C. Y. 2010 Adhesion of a fibrillar interface on wet and rough surfaces. *J. Adhes.* **86**, 39–61. (doi:10.1080/00218460903417834)

Waters, J. F. & Guduru, P. R. 2010 Mode-mixity-dependent adhesive contact of a sphere on a plane surface. *Proc. R. Soc. A* **466**, 1303–1325. (doi:10.1098/rspa.2009.0461)

Waters, J. F., Lee, S. & Guduru, P. R. 2009 Mechanics of wavy surface adhesion: JKR–DMT transition solution. *Int. J. Sol. Struct.* **46**, 1033–1042. (doi:10.1016/j.ijsolstr.2008.10.013)

Waters, J. F., Gao H. J. & Guduru, P. R. In press. On adhesion enhancement due to concave surface geometries. *J. Adhes.*

Yao, H., Della Rocca, G., Guduru, P. R. & Gao, H. 2008 Adhesion and sliding response of a biologically inspired fibrillar surface: experimental observations. *J. R. Soc. Interface* **5**, 723–733. (doi:10.1098/rsif.2007.1225)